Supporting Information for

Tailor plasmons in pentacene/graphene heterostructures with interlayer electron transfer

F. Hu[1,2]*, M. Kim[1,2]*, Y. Zhang[3], Y. Luan[1,2], K. M. Ho[1,2], Y. Shi[3], C. Z. Wang[1,2]†, X. Wang[3]†, Z. Fei[1,2]†

[1]Department of Physics and Astronomy, Iowa State University, Ames, Iowa 50011, USA
[2]U.S. DOE Ames Laboratory, Iowa State University, Ames, Iowa 50011, USA
[3]National Laboratory of Solid State Microstructures, School of Electronic Science and Engineering and Collaborative Innovation Center of Advanced Microstructures, Nanjing University, Nanjing 210093, China

* These authors contributed equally to this work.

† C.Z.W. (wangcz@ameslab.gov); X.W. (xrwang@nju.edu.cn); Z.F. (zfei@iastate.edu)

List of contents

1.   Experimental details

To perform nano-infrared (IR) imaging studies of the pentacene/graphene heterostructures, we employed the scattering-type scanning near-field optical microscopy (s-SNOM). Our s-SNOM apparatus (Neaspec GmbH) is based on an atomic force microscope (AFM) operating in the tapping mode. Measurements were acquired at an AFM tapping frequency of $\Omega = 270$ kHz and a tapping amplitude of about 60 nm. As illustrated in Figure 1a, we utilized a metalized AFM probe, which is illuminated by a p-polarized mid-IR beam from a continuous-wave CO_2 laser (Access Laser). In our s-SNOM measurements, we used Arrow-NCPt probes from NanoAndMore. The radius of tip apex of these probes is about 25 nm that defines the spatial resolution of the s-SNOM. The standard observable of an s-SNOM experiment is complex scattering signal demodulated at

the nth ($n = 3$ in the current work) harmonics of the AFM tip oscillation. We discuss mainly the amplitude part of the signal that is enough to describe the plasmonic responses of the samples.

Our pentacene/graphene vdW heterostructures were prepared by physical vapor transport deposition of uniform pentacene molecular layers on graphene. The heterostructure samples are sitting on the standard silicon wafers with 300-nm-thick thermal oxide on the top. The samples that we studied in this work include bare graphene, and one-layer (1L), two-layer (2L), three-layer (3L) and four-layer (4L) pentacene on graphene, determined by accurate AFM measurements (Figure S1).

2.   Additional s-SNOM imaging data

In Figures S2 and S3, we present the excitation energy (E) dependent nano-IR amplitude images of graphene, 1L pentacene on graphene, and 2L pentacene on graphene. Here the IR amplitude is normalized to that of the SiO_2 substrate. From Figures S2 and S3, one can see that the IR contrast between the samples and the SiO_2 substrate shows a clear evolution with energy. This is mainly due to the increase of the substrate signal as E approaches the surface phonon resonance of SiO_2 at around 140 meV. Moreover, the fringe period or the fringe width of the samples shrinks with increasing laser energy, indicating smaller plasmon wavelength. This is consistent with the dispersion properties of graphene plasmons (Figure S5). In all laser energies, there is a small signal difference between bare graphene and 1L pentacene on graphene and a larger contrast between 1L and 2L pentacene on graphene. This is consistent with the results discussed in the main text (Figures 1-3).

Figure S4a,b present the nano-IR imaging data of two heterostructure samples at an excitation energy of $E = 110$ meV. Sample 1 is the one that we extensively studied in the main text. Sample 2 is from a different wafer and it also contains bare graphene and 1L to 4L pentacene on graphene. Note that the excitation energy used here is slightly lower than that used in Figures 1 and 2 in the main text (116 meV). Here we compare the general signal contrast of different sample areas, which show good consistency among the two samples. For quantitative comparison, we plot in Figure S4c the average IR amplitude at the sample interior versus the number of pentacene layers (0 layer corresponds to bare graphene). Here one can see that the general trend of the signal evolution with layer thickness is consistent in the two heterostructure samples. There is a slight difference in 1L pentacene on graphene, which is possibly due to the degradation of 1L pentacene on sample 2 that leads to nonuniform signal distributions (Figure S4b).

3. Numerical modeling of the plasmon fringe profiles

To model the fringes profiles of plasmons confined inside graphene or pentacene/graphene heterostructures, we model our AFM tip as an elongated metallic spheroid (see Figure 3a in the main text): the length of the spheroid is $2L$ and the radius of curvature at the tip ends is a. Here, a is set to be 25 nm according to the manufacturer and L is set to be 500 nm and it is not a very sensitive parameter so long as $L \gg a$. The scattering amplitude s (before demodulation) scales with the total radiating dipole p_z of the spheroid. Therefore, to fit the line profiles perpendicular to the fringes inside samples, we need to calculate p_z at different spatial coordinates (x, z) of the lower end of the AFM tip. Here, x is the in-plane coordinate perpendicular to samples and z is the out-of-plane coordinate perpendicular to the sample surface. By calculating p_z at different z, we can perform 'demodulation' of the scattering amplitude s and get different harmonics of the scattering signal and calculating p_z at different x allows us to plot the modeling profiles of IR amplitude. In all our simulations, we assume no position dependence in the y-direction for simplicity. The

dielectric constants of SiO_2 used in the calculations are adopted from literature.[1] The dielectric constants of pentacene layers (ε_{ab}, ε_c) used in the calculations given in Section 6 below. The key modeling parameters for graphene are the plasmon wavelength (λ_p) and damping rate (γ_p). By fitting the experimental plasmon fringe profiles (Figure 2f-j in the main text), we can determine accurately λ_p and γ_p based on the experimental data (Figure 3b,c in the main text).

4. Calculations of the plasmon wavelength

In order to determine the Fermi energy (E_F) of graphene, we need to calculate λ_p theoretically and then compared to the experimental result obtained from fringe profile fitting (see the section above). For that purpose, we first compute the plasmon dispersion colormaps (Figure S5) by evaluating numerically the imaginary part of the reflection coefficient $Im(r_p)$ for the entire pentacene/graphene/substrate heterostructure system by using the transfer matrix method. These colormaps reveal the photonic density of states (DOS), and the plasmonic mode appears as a bright curve revealed by the colormaps. Such a dispersion calculation method has been widely applied in the studies of graphene plasmons and other types of polaritons. The optical conductivity of graphene is obtained by the Radom phase approximation methods (see Ref. 11 in the main text). The dielectric constants of pentacene layers used in the calculations given in Section 6 below. The dielectric constants of SiO_2 used in the calculations are adopted from literature.[1] Based on the calculated dispersion colormaps, we can determine the plasmon wavevector q_p and hence the plasmon wavelength $\lambda_p = 2\pi/q_p$ at any excitation energy. The dispersion colormaps shown in Figure S5 are calculated with different choices of E_F values shown in Figure 3d in the main text. The λ_p values read out from these colormaps match well the λ_p results determined through fringe profile fitting (Figure 2 in the main text), which confirms the validity of E_F values shown in Figure 3d.

5. DFT calculation methods and results

We performed first-principles electronic structure calculations based on density functional theory (DFT) using Vienna *ab initio* simulation package (VASP).[2,3] We employed the projector augmented wave method[4] and a plane-wave basis set with 400 eV energy cutoff. For the exchange-correlation functional, we used Perdew-Burke-Ernzerhof (PBE) functional[5], and a total of 5×2×1 k point meshes were used. We included the van der Waals energy using the DFT-D3 method.[6] In our slab calculations for the pentacene thin films, we used sufficiently thick vacuum regions (> 23 Å) to prevent the unwanted interactions between periodic images. We considered the structural model of pentacene layers that consist flat-lying wetting layer (WL) on graphene, the inclined one layer (1L) and the standing two (2L) and three layers (3L) (Figure S6).[7] The dielectric matrix was determined using density functional perturbation theory. In Figures S7 and S8, we presented the calculated band structures of pentacene layers and their potential energy line profiles taken along the vertical direction. From these calculations, we can determine the ionization potential (IP) of all pentacene layers (Table 1 in the main text).

Due to the self-interaction error, the conventional DFT calculations with local density approximation (LDA) or generalized gradient approximation (GGA) are not supposed to give accurate valence band energies, which in turn results in underestimated IP values.[8] Therefore, we performed the GW calculation (in the GW_0 level) that is expected to give a reasonable value for the IP. Due to the large computational cost, we used the approximation where we estimate the shift of the valence band maximum by that of the highest valence band energy at the Γ point of the Brillouin zone ($\Delta_{VB,\Gamma}$) in the 3D bulk pentacene crystal (Figure S9a). In the GW calculation of the

bulk pentacene, we used 2×2×1 k point meshes. We considered further correction coming from limited number of empty bands (Δ_{eb}). Specifically, we estimated the valence band energy with the infinite number of the empty bands ($N_{eb} = \infty$) included in the calculation by fitting the results of a series of different N_{eb} to the formula A/N_{eb} + B.

The results of both corrections are shown in Figure S9b,c, respectively. We denoted the sum of the two correction terms by Δ_{GW} (i.e., $\Delta_{GW} = \Delta_{VB,\Gamma} + \Delta_{eb}$). The total GW correction is as large as $\cong 0.96$ eV. After corrections, the IPs of thin pentacene layers are calculated to be 5.72 eV, 4.95 eV, 4.78 eV, and 4.78 eV for WL, 1L, 2L and 3L pentacene, respectively (Table 1 in the main text). These results are consistent with previous experiments.[9] Based on the calculation results, we conclude that the IP of pentacene is solely dependent on the orientation angle of pentacene molecules. Therefore, we expect that IPs of thicker pentacene layers (4L or above) are all about 4.78 eV.

6. Dielectric constants of pentacene

The dielectric constants of pentacene layers we used for the fringe profile modeling and dispersion calculations are also from DFT calculations. With DFT, we calculated the static dielectric constants of pentacene layers with different thicknesses. It is known from the previous study[10] that pentacene has a flat dielectric response up to the visible region when it is away from the strong vibrational modes of pentacene (the nearest strong resonance is at about 112 meV with a resonance width of 0.4 meV). Therefore, it is appropriate to use the static dielectric constants for calculations in the mid-infrared region. The calculated in-plane dielectric constants (ε_{ab}) for 1L, 2L and 3L pentacene are about 2.1, 2.6 and 2.7, respectively. The out-of-plane dielectric constants (ε_c) for 1L, 2L and 3L pentacene are about 1.3, 2.0 and 2.6, respectively. Both ε_{ab} and ε_c increase with pentacene thickness and they are trending towards the value for bulk pentacene films: $\varepsilon_{bulk} \approx 3.0$.[10] For 4L pentacene, we used dielectric constants of 3L pentacene as an approximation. The calculated λ_p only varies a little (~1.5%) even using $\varepsilon_{bulk} \approx 3.0$ for 4L pentacene. There is in fact a small ab-plane anisotropy (about 1%, 5% and 12% for 1L, 2L and 3L pentacene, respectively) in the dielectric constants according to our calculations, but it only causes tiny variations to λ_p (about 0.05%, 0.3% and 0.8% for 1L, 2L and 3L pentacene, respectively) due to the nanoscale thicknesses of the pentacene layers. Therefore, we used averaged ab-plane dielectric constants in our calculations ($\varepsilon_{aa} + \varepsilon_{bb}$)/2.

References for the Supporting Information
1. Palik, E. D. Handbook of Optical Constants of Solids. Academic Press (2012).
2. Kresse, G.; Hafner, J. *Phys. Rev. B* **1993**, 47, 558.
3. Kresse, G.; Furthmüller, J. *Phys. Rev. B* **1996**, 54, 11169.
4. Blöchl, P. E. *Phys. Rev. B* **1994**, 50, 17953.
5. Perdew, J. P.; Burke, K.; Ernzerhof, M. *Phys. Rev. Lett.* **1996**, 77, 3865.
6. Grimme, S.; Antony, J.; Ehrlich, S.; Krieg, H. *J. Chem. Phys.* **2010**, 132, 154104.
7. Zhang, Y.; Qiao, J.; Gao, S.; Hu, F.; He, D.; Wu, B.; Yang, Z.; Xu, B.; Li, Y.; Shi, Y.; Ji, W.; Wang, P.; Wang, X.; Xiao, M.; Xu, H.; Xu, J.-B.; Wang, X. *Phys. Rev. Lett.* **2016**, 116, 016602.
8. Jiang, H.; Shen, Y.-C. *J. Chem. Phys.* **2013**, 139, 164114.
9. Yoshida, H.; Yamada, K.; Tsutsumi, J.; Sato, N. *Phys. Rev. B* **2015**, 92, 075145.
10. Schubert, M.; Bundesmann, C.; Jacopic, G.; Maresch, H.; Arwin. H. *Appl. Phys. Lett.* **2004**, 84, 200-202.
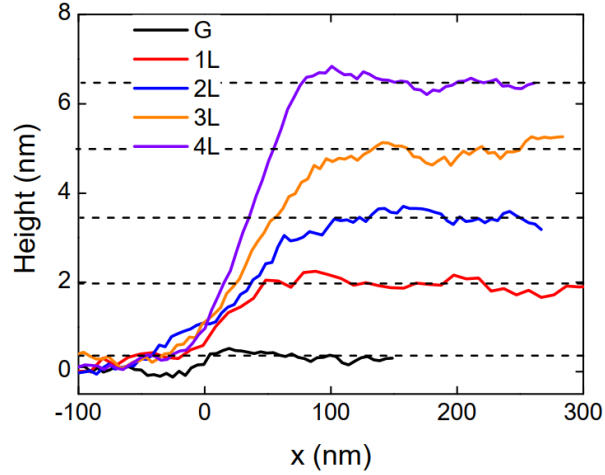
Figure S1. The AFM topography profiles of graphene (G) and 1L to 4L pentacene on graphene extracted from Figure 1b in the main text. Here the 0 pentacene layer corresponds to bare graphene.
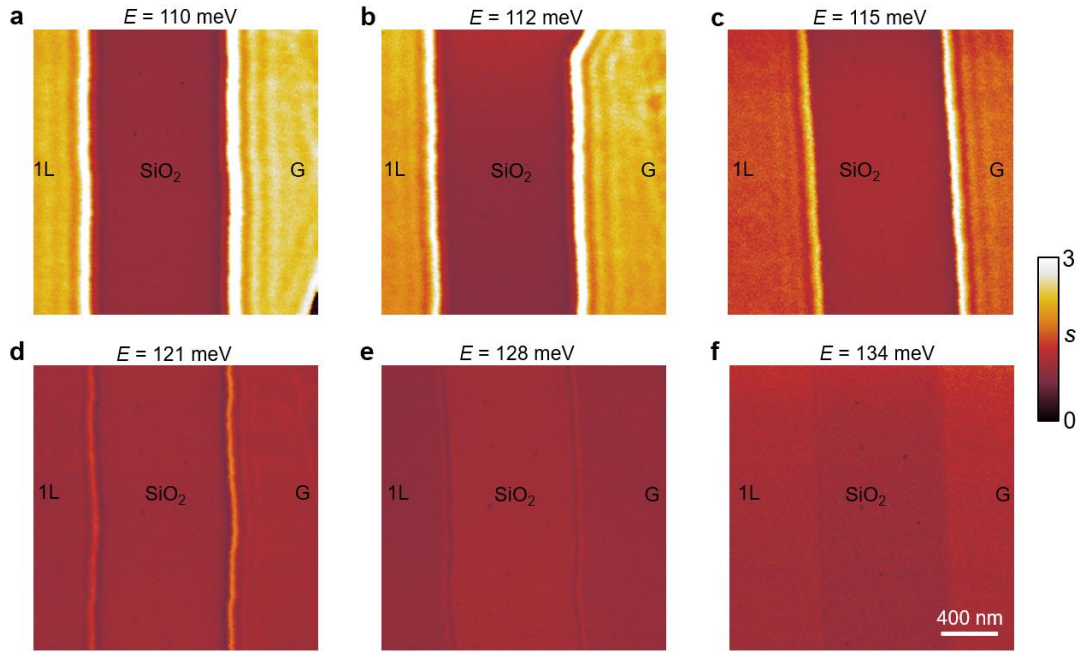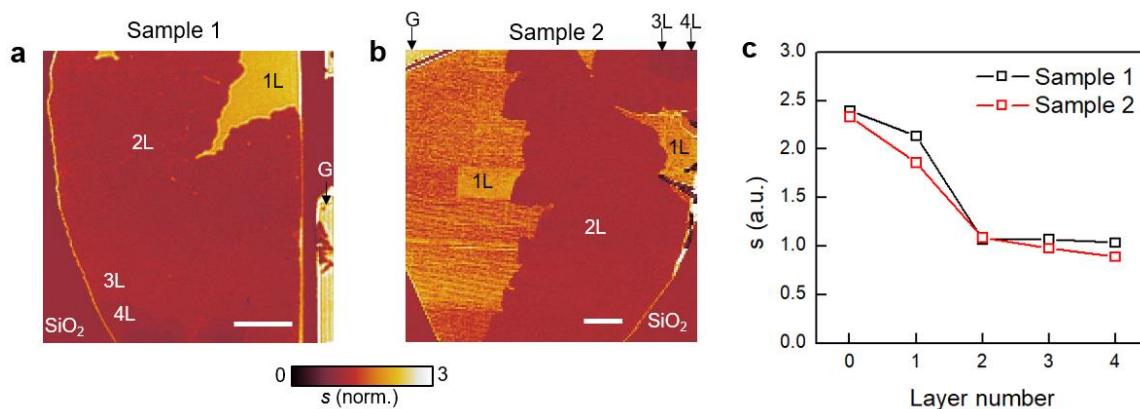

Figure S2. Excitation laser energy dependent nano-IR imaging data of bare graphene (G) and 1L pentacene on graphene. Here we plot the IR amplitude normalized to that of the SiO_2 substrate.
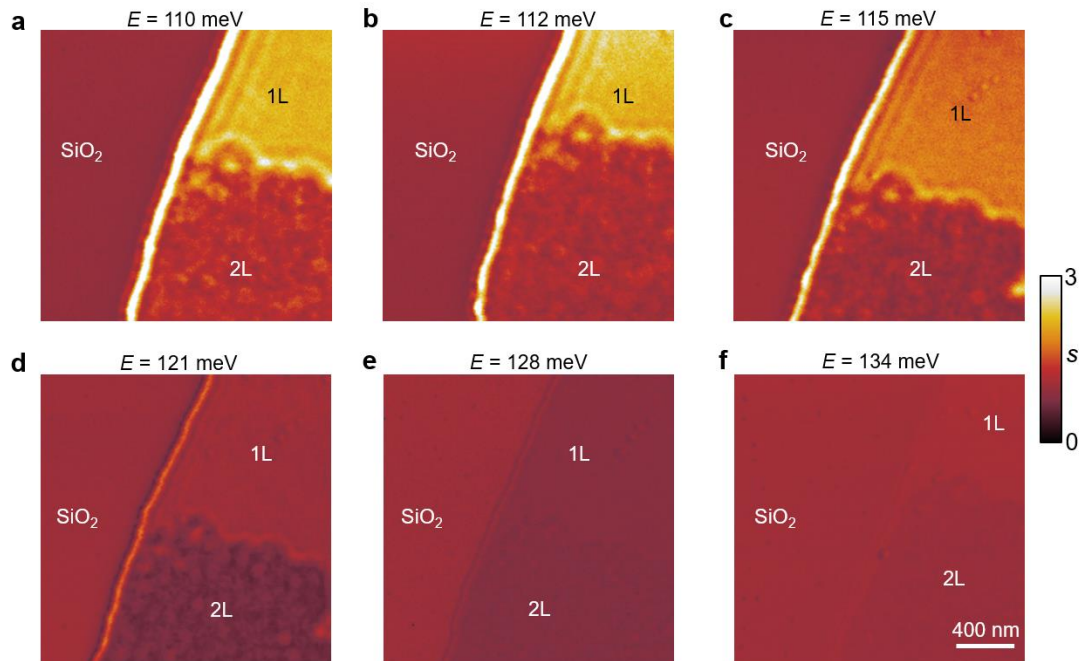
Figure S3. Excitation laser energy dependent nano-IR imaging data of 1L and 2L pentacene on graphene. Here we plot the IR amplitude normalized to that of the SiO_2 substrate.


Figure S4. a,b, Nano-IR imaging of two samples at an excitation energy of 110 meV (slightly lower energy compared to that used in Figure 1 and 2 in the main text). Sample 1 is the sample we studied extensively in the main text. Sample 2 is a different sample on a different wafer. Scale bars: 2 μm. **c**, The IR amplitude signals of the two samples taken from **a,b** versus the number of pentacene layers.
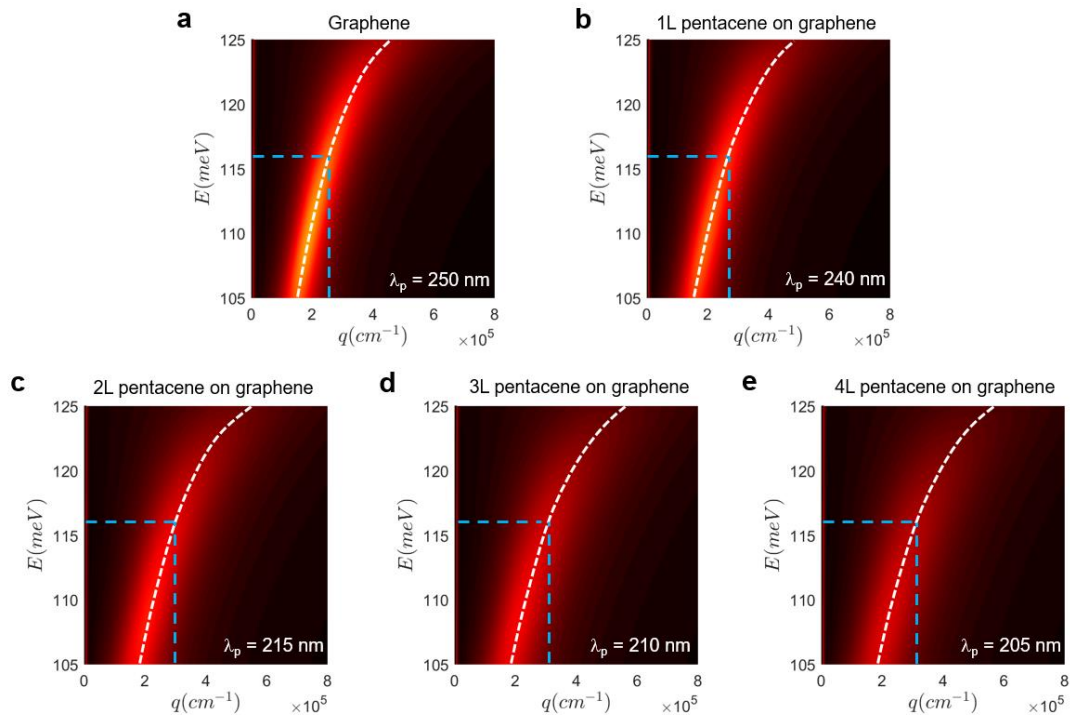
Figure S5. Calculated dispersion colormaps of bare graphene (**a**) and pentacene layers with different thicknesses on graphene (**b**-**e**). The white dashed curves mark the dispersion relation of graphene plasmons revealed by the color maps. The horizontal and vertical blue dashed lines mark the excitation energy (E = 116 meV) and corresponding plasmon wavevector determined by the dispersion diagrams.
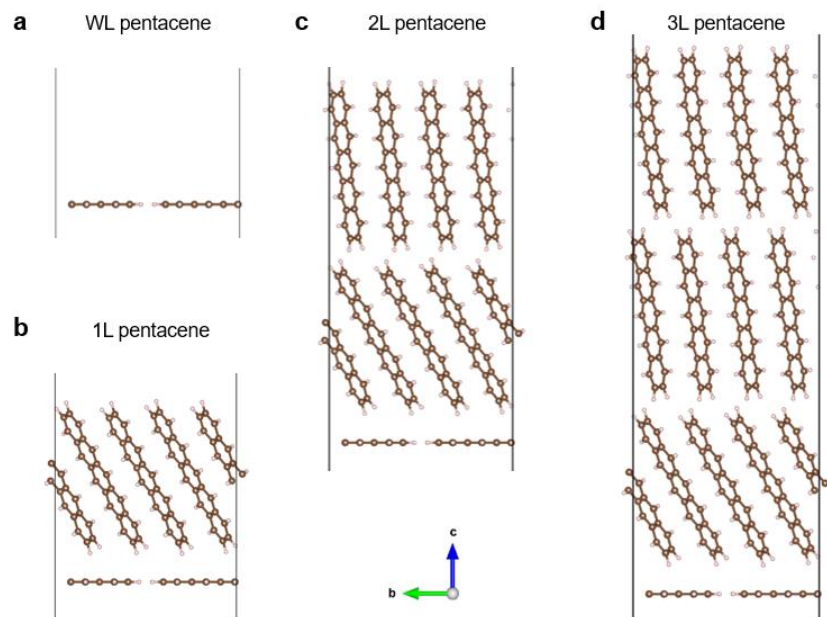
Figure S6. Atomic structures of different pentacene layers that we constructed for DFT calculations.
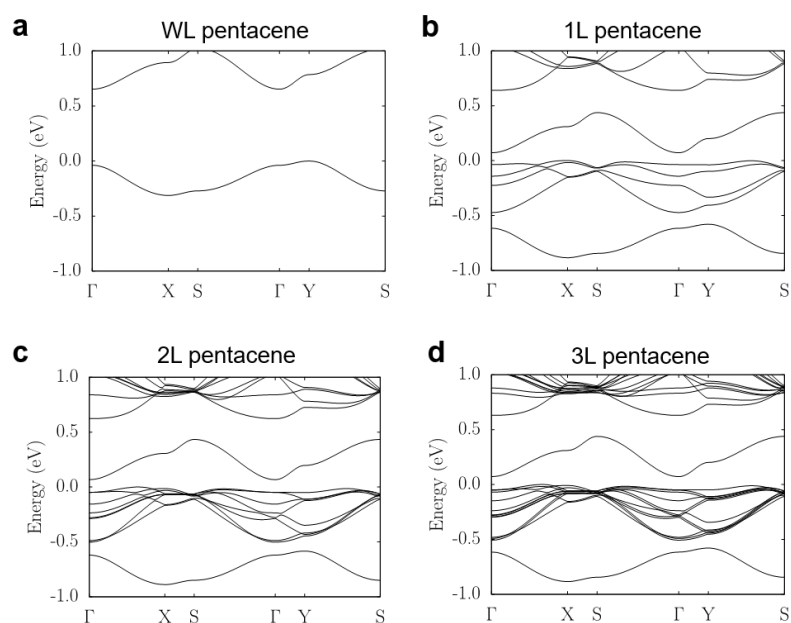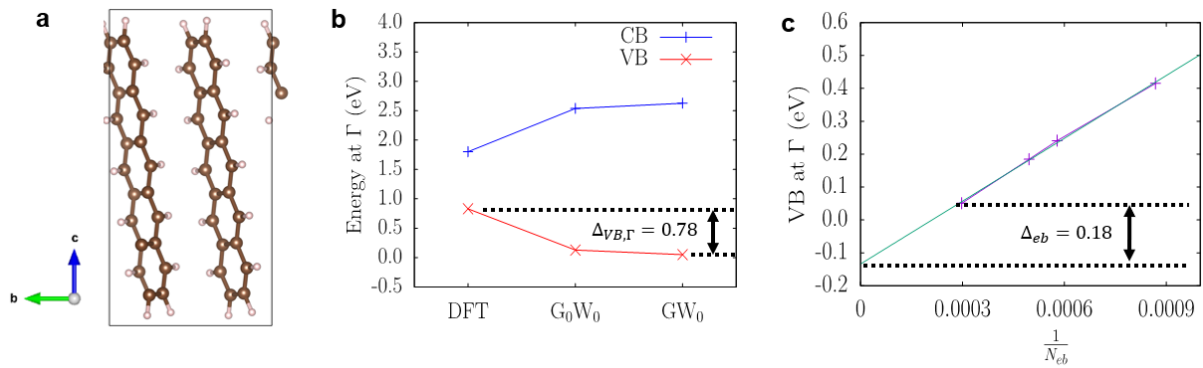
Figure S7. The DFT calculations of band structures of WL, 1L, 2L and 3L pentacene. In all the plots, the band structures are shifted on purpose to set the valence band maximum right at 0 eV.
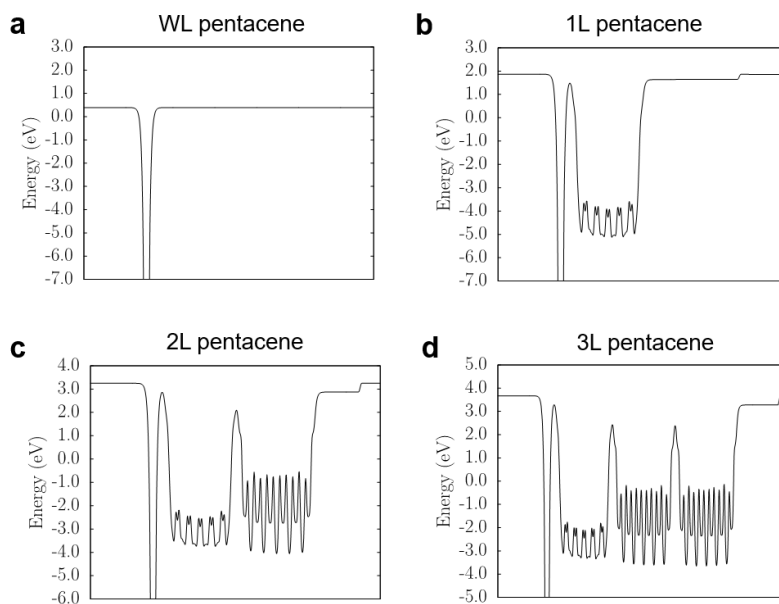
Figure S8. The DFT calculations of potential energy profiles of WL, 1L, 2L, and 3L pentacene along the *c* axis (perpendicular to the pentacene layers).

Figure S9. a, Unit cell of bulk pentacene that we used for GW calculations. **b,** Shift of the valence band maximum by that of the highest valence band energy at the Γ point of the Brillouin zone ($\Delta_{VB,\Gamma}$). **c,** Correction coming from limited number of empty bands (Δ_{eb}).